Submitted to *J. Geophys. Res. Atm.* July 11, 2002. Revised October 24, 2002. Accepted October 28, 2002.

Tropospheric Aerosol Impacts on Trace-Gas Budgets through Photolysis

Huisheng Bian and Michael J. Prather

Department of Earth System Science, University of California at Irvine

Toshihiko Takemura

Research Institute for Applied Mechanics, Kyushu University, Fukuoka, Japan

Abstract.
Aerosols affect the global budgets of O_3, OH and CH_4 in part through their alteration of photolysis rates and in part through their direct chemistry interactions with gases (a.k.a. "heterogeneous chemistry"). The first effect is evaluated here with a global tropospheric chemistry transport model using recently developed global climatologies of tropospheric aerosols: a satellite-derived aerosol climatology over the oceans (AVHRR) and a model-generated climatology for land plus oceans (CCSR). Globally averaged, the impact of aerosols on photolysis alone is to increase tropospheric O_3 by 0.63 DU and increase tropospheric CH_4 by 130 ppb (via tropospheric OH decreases of 8%). These greenhouse gas increases lead to an aerosol indirect effect (counting both natural and anthropogenic aerosols) of +0.08 W/m^2. Although the CH_4 increases are of course global, the changes in tropospheric OH and O_3 are mainly regional with largest impacts in northwest Africa for January and in India and southern Africa for July. The influence of aerosols is greater in July than in January, greater in the Northern Hemisphere than in Southern Hemisphere, as expected for pollution sources in the Northern Hemisphere. The predominant impact is due to the aerosols over land, aerosols over ocean contribute less than a third to globally integrated changes.

1. Introduction

Studies of aerosol influence on tropospheric photolysis and chemical budgets have been conducted in field campaigns and model simulations for individual stations and over regional scales [*Dickerson et al.*, 1997; *He and Carmichael*, 1999; *Balis et al.*, 2001]. These impacts, however, need to be integrated on a global scale and over decades (i.e., the relaxation time of the CH_4-like mode in global tropospheric chemistry) to assess their importance in trace-gas budgets and the greenhouse gas forcing of climate. This gap in the globally integrated impacts of aerosols on photochemistry is due in part to the fact that a global climatology of aerosol properties in not quite ready [*Dubovik et al.*, 2002; *Clarke and Kapustin*, 2002] and in part to the difficulty in developing an efficient global tropospheric chemistry model that readily includes the effects of clouds and aerosols on photolysis rates. Aerosol properties and distributions have recently been the focus of intensive investigations through model simulations [*Penner et al.*, 2002; *Chin et al.*, 2002; *Takemura et al.*, 2002], satellite retrievals [*Stowe et al.*, 1997; *Mishchenko et al.*, 1999a; *Higurashi et al.*, 2000; *Torres et al.*, 2002], and field campaigns [*Ansmann et al.*, 2000; *Bates et al.*, 2001; *Holben*, 2002]. These new aerosol data sets and a newly developed on-line photolysis model in the UC Irvine (UCI) global chemistry-transport model (CTM) [*Wild et al.*, 2000; *Bian and Prather*, 2002] make it possible to evaluate the impact of aerosol scattering and absorption on the greenhouse gases CH_4 and O_3.

Ideally, in this evaluation we would use a global, observationally based, and hence satellite-derived, aerosol clima-

tology, for example, the aerosol products retrieved from the AVHRR channel 1 and 2 radiance data [*Mishchenko et al.*, 1999a; *Mishchenko*, 2000]. While these two-channel data provide aerosol optical thickness (AOT) and one size parameter, they lack key information on the vertical distribution, the absorptive properties, and the scattering phase function in the ultraviolet-visible region, all of which control the aerosol influence on photochemistry. Further, this product is currently available only over the oceans since retrievals over land are less certain due to variations in surface reflectivity [*Knapp and Stowe*, 2002]. It is expected that in time the EOS-Terra instruments will be able to develop aerosol climatologies that provide much of this key data [*Diner et al.*, 2001; *Hook et al.*, 2001]. As a surrogate for this observational aerosol climatology, we take the aerosol simulations from the Center for Climate System Research (CCSR) [*Takemura et al.*, 2000]. The detailed CCSR climatology provides January and July monthly averages that separate sulfate, sea-salt, dust and carbonaceous (organic plus black) aerosols. Given the atmospheric abundances, size distributions, and refractive indices for the different aerosol types in three dimensions, it is easy to calculate the optical depth and scattering / absorption properties in each CTM layer. We compare the CCSR and AVHRR climatologies directly with an ocean-only aerosol chemical calculation in which the AVHRR climatology adopts the aerosol optical properties but not the AOT of the CCSR 3-D product.

The two aerosol climatologies are described and compared in Section 2. The UCI CTM and the methodology of the different chemical simulations are presented in Section 3. we analyze the impact of aerosols on the tropospheric burdens of O_3, OH, CH_4, and some odd-nitrogen species in Section 4. In the concluding Section 5 we estimate that the photolytic effect of aerosols (natural plus anthropogenic) on the greenhouse gases CH_4 and O_3 is +5 to +10% of the change since the pre-industrial era and amounts to +0.08 W/m^2.

2. Aerosol Climatologies

An aerosol climatology over oceans has been derived from the AVHRR satellite radiances at channel 1 (λ=650 nm) and channel 2 (λ=850 nm) [*Mishchenko et al.*, 1999a] using monthly averages from the period February 1985 through October 1988. This two-channel algorithm works only over oceans (uniformly dark surfaces) and provides more accurate and less biased retrievals of the AOT than one-channel algorithm. It also provides some information on aerosol size through the Angstrom parameter, defined as the exponential dependence of AOT on wavelength between the two channels. Figure 1 shows the total AOT at 550nm for the AVHRR ocean aerosol in January and July. No consolidated satellite climatology for land-plus-ocean aerosol was available from the Global Aerosol Climatology Project (GACP) for this study. The CCSR model simulations [*Takemura et al.*, 2000] of AOT for each aerosol type (dust, carbonaceous, sulfate, and sea-salt) are available only for January and July. Figure 2 shows the CCSR 550 nm AOT in both January and July for the sum of all aerosol types.

A summary comparison of the two aerosol climatologies is given in Table 1 where the ocean-only AOT for July is averaged over regions and CCSR AOT is further separated by aerosol type. Differences appear largest over the remote ocean where the CCSR predicts about a factor of 2 less than AVHRR retrievals. *Kinne et al.* [2002] present a global comparison among seven models, three satellite data sets, and the AERONET data, focusing on monthly averages of aerosol properties. They report that model simulations are usually smaller than satellite derived values, especially when comparing to TOMS data and AVHRR data in remote regions. Furthermore, they point out that low predicted AOT in remote region by CCSR is likely caused by either weak transport or strong removal of dust, carbonaceous, and sulfate aerosols combined with weak mass extinction efficiency of sea salt. Over oceanic regions affected by land aerosol sources the CCSR AOT is equivalent or slightly higher, and over the northern Indian Ocean it is more than twice the AVHRR AOT. In these regions, near combustion and biomass burning sources, the CCSR aerosol extinction for carbonaceous aerosols (including organic and black) is much greater than in remote regions. Although the CCSR AOT in remote ocean is much smaller than the AVHRR, the areas affected by land sources have a larger weighting in estimating the global mean ocean AOT. Thus, the global oceanic mean AOT from CCSR is only slightly less than the AVHRR retrieval in July.

The CCSR climatology specifies the 3-D aerosol extinction at 550 nm by type, but we must still adopt an aerosol model (size distribution and index of refraction) to derive the optical properties used to calculate photolysis rates [*Wild et al.*, 2000]. Specifically, the single scatter albedo and the first 7 coefficients in the Legendre expansion of the scattering phase function for ultraviolet and visible wavelengths (300 - 600 nm) are needed. For each CCSR type (sulfate, carbonaceous, dust, and sea salt) we adopt an index of refraction (n, wavelength independent) and log-normal size distribution (r_g and σ) based on atmospheric measurements [*Twitty and Weinman*, 1971; *Volz*, 1972; *Ward et al.*, 1973; *Grams et al.*, 1974; *Hsu et al.*, 1999; *Ji et al.*, 2000; *Diaz et al.*, 2001]. This model is summarized in Table 2 along with the optical properties as a function of wavelength calculated from Mie theory: the single scatter albedo (ω_0) and Legendre expansion of the scattering phase func-

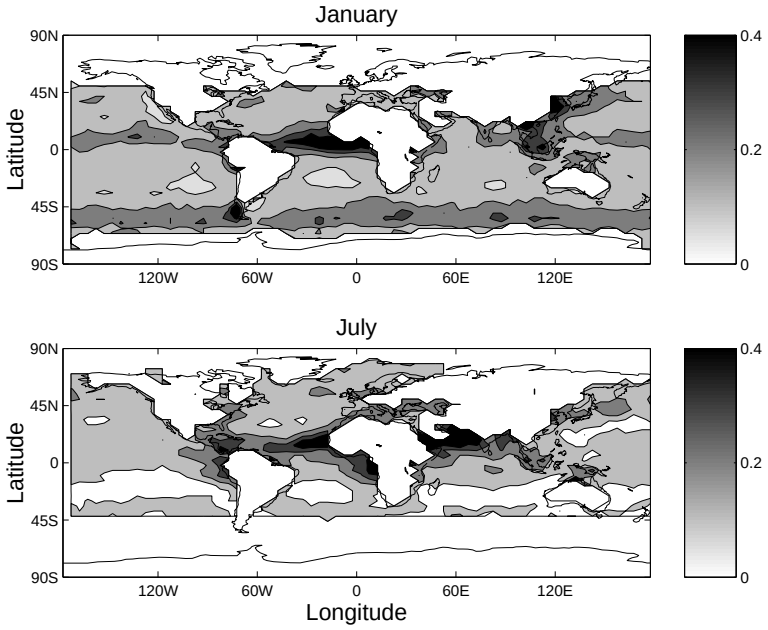

Figure 1. Aerosol optical thickness at 550nm over oceans averaged over January and over July from the AVHRR climatology *Mishchenko et al.* [1999a].

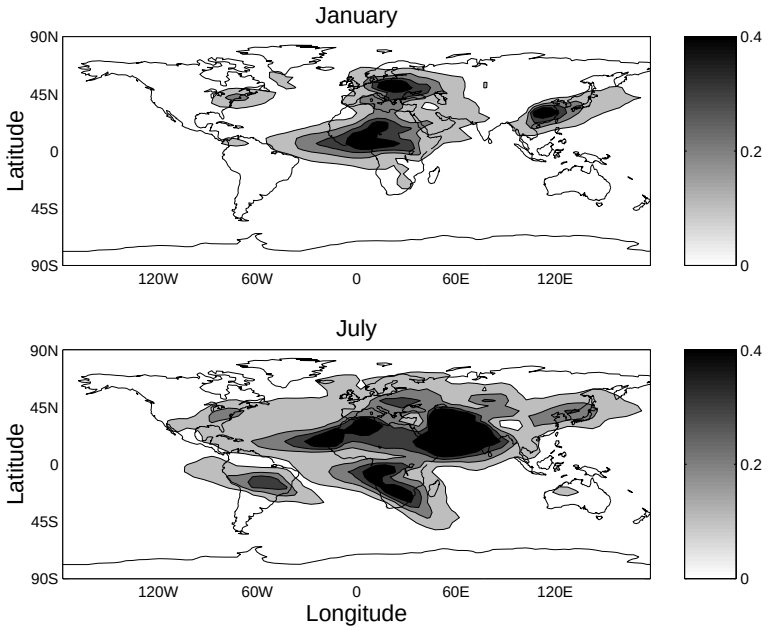

Figure 2. Total aerosol optical thickness (sum of sea salt, sulfate, dust and carbonaceous) at 550nm averaged over January and over July for CCSR model *Takemura et al.* [2000].

tion (ω^i, i=0,...,7). Also given are diagnostic quantities, the extinction efficiency (Q, mean extinction cross-section over cross-sectional area) and the effective radius (r_{eff}, area weighted mean radius). The detailed properties at 999 nm are not important in photolysis but are included because Fast-J can then scale AOT reported at 1 micron (e.g., strato-

Table 1. The comparison of ocean AOT at 550 nm for July between satellite AVHRR retrieval by *Mishchenko et al.* [1999a] and the CCSR model generated by *Takemura et al.* [2000].

Ocean	AVHRR	CCSR				
Regions	Total	Total	carbonaceous	sulfate	sea-salt	dust
Global oceans	0.16	0.13	0.037	0.036	0.016	0.044
NH oceans	0.19	0.17	0.026	0.057	0.012	0.077
SH oceans	0.12	0.085	0.05	0.010	0.021	0.004
E.Pacific (NH)	0.14	0.048	0.006	0.023	0.010	0.008
W.Pacific (NH)	0.14	0.086	0.013	0.049	0.009	0.014
E.Pacific (SH)	0.11	0.045	0.016	0.006	0.021	0.002
Indian (SH)	0.09	0.064	0.028	0.007	0.024	0.006
Atlantic (Equ)	0.29	0.32	0.14	0.042	0.015	0.13
Pacific / E.Asia	0.16	0.22	0.046	0.12	0.008	0.046
Indian (NH)	0.43	1.08	0.059	0.10	0.022	0.90

spheric sulfate aerosols). Note that we use our aerosol model (i.e., Q(λ)) rather than the Angstrom coefficient to calculate the AOT climatologies from 550 nm to the critical wavelength range for tropospheric photochemistry (300 - 400 nm). In combining extinction from different aerosol types (and sometimes clouds) in a CTM layer, we assume an external mixture.

The AVHRR ocean climatology is only two-dimensional and lacks both vertical distribution and speciation. We must make several assumptions to use it in the CTM. For speciation, we assume an external mixture and use the CCSR climatology to calculate an average index of refraction over each ocean grid cell in the CTM, weighting the indices of refraction in Table 2 by the CCSR 550 nm AOT for each type. We calculate the optical properties for each grid cell by combining this mean index of refraction with a modified bimodal log normal distribution using the AVHRR-specific parameterization [*Mishchenko et al.*, 1999b; *Higurashi et al.*, 2000] that includes variation in the fraction of large particles as a function of AOT. The vertical distribution of aerosol extinction for the AVHRR climatology was set proportional to the local water vapor density in the CTM.

Aerosol refractive index determines the single scattering albedo and is a key parameter controlling photolysis rates. It must be regarded as a major uncertainty in this investigation. We adopt a smaller imaginary refractive index (0.003) than previous value (0.005) for sea salt recommended by recent study [I. Geogdzhayev, 2000, personal communication]. A sensitivity study using AVHRR climatology examines a range in aerosol absorption. Both carbonaceous aerosols and desert dust absorb strongly in the wavelength range of 300 to 400 nm, while sea salt and sulfate aerosols absorb very little. Since we chose a wavelength-independent index of refraction, we keyed this value for dust aerosol to give a single scattering albedo in the photochemical region (300-400 nm) of about 0.66. According to recent studies on mineral dust over the tropical north Atlantic Ocean, the single scattering albedo of dust at wavelengths less than 400 nm can be less 0.6, but it increases rapidly for wavelengths greater than 550 nm [*Savoie et al.*, 2000; *Ji et al.*, 2000]. Some other studies [*Diaz et al.*, 2001; *Kaufman et al.*, 2001; *Dubovik et al.*, 2002] about single scattering albedo over or toward the photochemical spectrum also support our standard model in Table 2. On the other hand, *He and Carmichael* [1999] give a single scattering albedo for Saharan dust as 0.77 (independent of wavelength) in their calculations of photolysis rates. Thus, we consider an alternative model of moderate dust absorption (mod-D) with a lower imaginary refractive index that raises the single scattering albedo at 300 nm from 0.62 (using the AVHRR size distribution and the CCSR index of refraction) to 0.72. *Hsu et al.* [1999] and *Twitty and Weinman* [1971] suggest three different refractive indices for carbonaceous aerosols to represent weak (single scattering albedo of 0.9 at 300-400 nm), moderate (0.8), and strong(0.5, the standard model) absorption depending on the fraction of black versus organic carbon. We combine the moderate dust absorption alternative with moderate and weak carbonaceous absorption to define two alternative models, mod-C and weak-C, with successively less absorption. Finally, we consider that all AOT over the ocean is sea salt with minimal absorption (0.95 at 300-400 nm).

3. Tropospheric Chemistry Simulations

The three-dimensional global chemical transport model at UCI can be driven by different meteorological fields. The

Table 2. Aerosol radiative properties adopted for CCSR types as a function of wavelength (λ) (see text). Carbonaceous includes both organic and black carbon. Q (extinction efficiency) and r_{eff} (area-weighted mean radius) are diagnostic and not used in photolysis calculations.

λ (nm)	Q	r_{eff}	ω^0	ω^1	ω^2	ω^3	ω^4	ω^5	ω^6	ω^7
Sulfate (n=1.45-.0037i, log-norm: r_g=90 nm σ=.6)										
300	2.7040	0.224	0.9702	2.212	2.829	2.764	2.568	2.213	1.861	1.554
400	2.3984	0.224	0.9749	2.198	2.683	2.525	2.181	1.774	1.381	1.079
600	1.6009	0.224	0.9770	2.101	2.410	2.066	1.639	1.203	0.863	0.612
999	0.7455	0.224	0.9738	1.898	1.958	1.460	1.015	0.651	0.416	0.260
Carbonaceous (n=1.80-0.30i, log-norm: r_g=140 nm σ=.37)										
300	2.8113	0.198	0.4943	2.363	3.152	3.389	3.249	2.892	2.400	1.919
400	2.9349	0.198	0.5104	2.213	2.635	2.524	2.088	1.601	1.124	0.755
600	2.7167	0.198	0.5224	1.933	1.861	1.394	0.884	0.497	0.268	0.133
999	1.7662	0.198	0.4726	1.483	1.100	0.537	0.226	0.078	0.027	0.009
Dust (A=1.5-.025i, log-norm: r_g=250 nm σ=.79)										
300	2.3972	1.182	0.6339	2.552	3.847	4.810	5.783	6.561	7.342	7.987
400	2.4507	1.182	0.6709	2.469	3.606	4.346	5.092	5.631	6.172	6.570
600	2.5593	1.182	0.7244	2.349	3.293	3.735	4.166	4.396	4.613	4.741
999	2.6365	1.182	0.7902	2.260	2.978	3.118	3.202	3.119	3.030	2.912
Sea-salt (n=1.5-.003i, log-norm: r_g=300 nm σ=.4)										
300	2.6056	0.452	0.9437	2.029	2.951	2.962	3.502	3.420	3.767	3.754
400	2.8618	0.452	0.9608	2.044	2.795	2.739	2.976	2.795	2.799	2.623
600	3.1537	0.452	0.9771	2.098	2.725	2.587	2.422	2.053	1.703	1.382
999	2.6244	0.452	0.9844	2.111	2.449	2.110	1.646	1.160	0.781	0.498

met-fields used in this study are from the Goddard Institute for Space Studies (GISS) general circulation model version II' that is run with a resolution of 4 ° latitude, 5° longitude and 9 vertical layers. These met-fields include 3-D (winds, temperature, water vapor, clouds, convection) and 2-D (boundary layer properties) data at 3-hour averages. The CTM resolution matches that of these GISS met-fields and includes an O_3-NOx-NMHC chemical scheme with 36 species, 88 chemical kinetic reactions, and 22 photolytic reactions [*Wild and Prather*, 2000; *Wild and Akimoto*, 2001; *Bian*, 2001]. Trace-gas emissions are based on the GEIA database [*Benkovitz et al.*, 1996] with updated totals from the IPCC third assessment [*Prather and Ehhalt*, 2001]. A first order rainout parameterization for soluble gases is used for large scale precipitation [*Giorgi and Chameides*, 1986], and scavenging in convective precipitation is built in to convective mass transport operator [*Bian*, 2001]. Dry deposition of gases is calculated with a resistance-in-series scheme [*Jacob et al.*, 1992]. Numerical solution for advection and convection conserves the second-order moments of tracer distribution (i.e., quadratics plus cross-terms). The UCI CTM has been applied previously to the simulations of both tropospheric and stratospheric chemistry and transport [*Prather et al.*, 1987; *Hall and Prather*, 1993; *Avallone and Prather*, 1997; *Jacob et al.*, 1997; *Hannegan et al.*, 1998; *Olsen et al.*, 2000; *McLinden et al.*, 2000]. The tropospheric model has been evaluated recently in several publications: tropospheric O_3 and CO, NOx/NOy species at Mauna Loa, and global PAN profiles in *Wild and Prather* [2000] and *Wild and Akimoto* [2001]; further O_3 and CO evaluations in IPCC 2001 [*Prather and Ehhalt*, 2001]; and updated radon and lead simulations in [*Bian*, 2001].

Aerosols are included here in the calculation of photolysis rates using the multiple-scattering fast-J scheme [*Wild et al.*, 2000; *Bian and Prather*, 2002] which explicitly accounts for aerosol and cloud optical properties. In each CTM layer the monthly mean aerosol extinction is combined with the 3-hour cloud optical depths form the met fields. Fast-J is computationally efficient and the radiation field as a function of wavelength is calculated throughout the entire column

hourly. Tropospheric photolysis is calculated from seven, variable-width wavelength bins between 289 and 850 nm. Atmospheric absorption and scattering include O_2 and O_3 absorption, Rayleigh scattering, water cloud and ice cloud absorption and scattering, and aerosol absorption plus scattering.

Calculating the impact of a perturbation to tropospheric chemistry alone would require several decades of continuous simulation to allow for CH_4 to respond. If stratospheric chemistry were included, this time would be centuries. For these exploratory studies, we restrict ourselves to tropospheric chemistry and use several approximations to calculate the aerosol impact. The CTM control case is run without aerosols. For some sensitivity studies, we use very short, two-month simulations: begin June 1 with the same initialization as the control run; impose different aerosol models; integrate through July 31; and diagnose the changes averaged over July. These simulations give us a quick look at the relative impact of differing assumptions, but the absolute numbers cannot be used quantitatively. While the one-month spin-up allows for O_3, OH, H_2O_2 and most odd-nitrogen species to come close to steady-state, the perturbation to other key gases like CO and C_2H_6 is still far from steady-state and their approach to steady-state will continue to change O_3 and OH. For our budget studies we complete a nineteen-month, full seasonal CTM simulation beginning July 1 Year 1 (from a much longer run) and ending Jan 31 Year 3. Due to the lack of a continuous climatology from CCSR we ran two perturbation budget studies: one with a perpetual January CCSR climatology and the other with a perpetual July. Examples of changes in trace gases and budgets are derived from Jan Year 3 (using January aerosols) and July Year 2 (using July aerosols). The minimum twelve-month spinup time of these runs allows for most chemically important trace gases, except CH_4, to settle close to steady state. These budgets are then used to project the steady-state CH_4 perturbation, including its feedback upon its own lifetime as per recent assessments [*Prather and Ehhalt*, 2001].

4. Results

Changes in tropospheric O_3 caused by the interaction of aerosols with the ultra-violet and visible radiation field are shown in Figure 3 for January and July. Results are plotted from the budget runs for the first 6 CTM model levels as CCSR aerosols minus control run for O_3 and divided by control run further for OH. Note that CH_4 is evolving slowly in these simulations and hence the change in O_3 does not include the effects of the CH_4 perturbation (diagnosed later) that would add about 0.4 ppb globally to these figures.

For tropospheric O_3 the inclusion of the aerosols leads to an increase of about +1 ppb over most of the globe, but regionally this change can vary from less than -15 to more than +2 ppb in January and from -10 to +3 ppb in July. In the low-aerosol regions, this increase is slightly large in the summer hemisphere. In regions with lower aerosol loading O_3 perturbations are between $\pm$ 2 ppb in both January and July; but in regions with high aerosol loading, particularly absorbing aerosol, O_3 abundances are suppressed by more than 2 ppb. This fits with previous studies reporting O_3 reductions in the lower atmosphere due to the presence of absorbing aerosols [*Jacobson*, 1998; *He and Carmichael*, 1999]. These O_3 reductions are largest and appear to be created in the lower troposphere. They are manifest in the upper troposphere and downwind by convective and advective transport. In our model the reduced O_3 occurs primarily over high-NOx, continental, ozone-producing regions and is driven by the general reduction in photolysis rates resulting in less photochemical formation of O_3. Over the low-NOx oceanic regions, O_3 is being destroyed by photochemistry [*Olson et al.*, 1997] and hence the presence of absorbing aerosols (e.g., over the tropical Atlantic) reduces this loss, resulting in O_3 increases of more than 2 ppb or more. On average, aerosols tend to reduce the photochemical loss of O_3 in the boundary layer and lead to the global background increase of less than 1 ppb. The largest ozone changes are coincident with dust (Sahara and Arabia) and biomass burning aerosols (South America and Africa). Note that O_3 loss over Europe in January is small even though aerosol loading is high (see Figure 2). In Europe the AOT is dominated by sulfate aerosol with very low absorptivity, and, further, the wintertime photochemical production of O_3 in mid-latitudes is low. In July with photochemical production in the continental boundary layer becoming important, aerosol scattering is seen to decrease O_3 over North America and Europe, although this effect does not impact much beyond the boundary layer.

Changes to tropospheric OH caused by aerosols are shown in Figure 4 for January and July. The global patterns are similar to those for O_3, but, interestingly, there are no regions of significant increase. Over most of the globe, OH decreases are less than 10%; however, tropospheric OH decreases by more than 30% over west Africa in January and by more than 50% over north Indian Ocean in July. In general, OH decreases are driven by reductions in ultraviolet photolysis of O_3 to form $O(^1D)$, the primary source of OH. Other photochemical changes augment this, for example, reductions in NO alter the balance between OH and HO_2, favoring the latter. In addition, decreases in OH have a positive feedback in that the resulting increases in CO lead to further OH decreases. As noted for O_3 above, the CH_4 perturbation in these runs is far ($> 90\%$) from steady state, and if we project

the CH_4 perturbation, there is an additional OH decrease of 2%. The OH decreases are larger and show more horizontal inhomogeneity in the lower troposphere than in the upper atmosphere, reflecting the rapid photochemical response of OH to local conditions. When only scattering is considered, as in Berntsen and Isaksen's [1997] study of the impact of clouds on upper tropospheric chemistry, the calculated OH abundances are larger above clouds than for clear-sky conditions. Thus, it is clear that aerosol absorption rather than scattering is driving these global OH decreases.

Sensitivity tests with only one-month spinup are used to assess the relative global importance of different aerosol models. The average July perturbations to the global burdens of tropospheric O_3, NO, NO_2, PAN, and OH following a June 1 initialization are summarized in Table 3. For the CCSR climatology, the aerosols over the oceans (70% of the surface) are responsible for only 20-40% of the total perturbation. The ocean-only climatologies of CCSR and AVHRR for July yield similar perturbations, although those of AVHRR are systematically larger as expected from their slightly larger AOTs. The importance of aerosol absorptivity is demonstrated with the ocean-only AVHRR sequence using different models for the refractive index (see discussion under aerosol model). Reducing the dust absorption by a third (mod-D) has little impact. By additionally reducing the carbonaceous absorptivity to a single scattering albedo of 0.8 (mod-C) and 0.9 (weak-C), the aerosol impact is reduced by a factor of three. Using a sea-salt model for all oceanic aerosols results in a negligible impact. Thus, the land aerosols dominate, and it is the absorptivity of the carbonaceous and dust aerosols that drives the changes in tropospheric photochemistry.

5. Projections and Conclusions

The budget lifetime of CH_4 in this CTM is 9.6 yr, and the e-fold time of a perturbation is about 14 yr [*Wild and Prather*, 2000]. We use this knowledge of the chemical modes and the CH_4 feedbacks diagnosed from many CTMs to project these aerosol perturbations to a steady state. Table 4 summarizes the increase in CH_4 lifetime, the decrease in tropospheric OH burden, and the increase in tropospheric O_3 burden for January and July budget runs as caused by aerosol impacts on photolysis. The northern summer dominates by more than a factor of 2. We estimate an annual average from these two months (e.g., a 5.6% increase in CH_4 lifetime) and use the IPCC 2001 results from an ensemble of CTMs [*Prather and Ehhalt*, 2001] to estimate the feedbacks when the CH_4 perturbation reaches steady state. These feedbacks augment the mean tropospheric OH perturbation by a factor of 1.4 and predict that the CH_4 abundance is about 130 ppb higher with aerosols than without. The tropospheric O_3 burden is greatly amplified by this increase in CH_4, from 0.25 to 0.63 DU. In summary, the impact of aerosols on photolysis alone is to increase tropospheric O_3 by about 1 ppb and to increase tropospheric CH_4 by about 130 ppb (via tropospheric OH decreases of about 8%). These greenhouse gas increases produce an increase in radiative forcing of about 0.08 W/m^2.

In this paper, we calculate global aerosol-photolysis coupling using a photolysis model (Fast-J) within the UCI CTM that couples aerosol and cloud layers. The results clearly show impacts at the 5-10 % level for global tropospheric chemistry, but regional perturbations can be as large as 50%, for example, in OH abundances. Perturbations are largest in the lower troposphere, over the continents, and generally in the summer hemisphere. This aerosol impact is dominated by the highly absorbing aerosols (carbonaceous and dust). The global results here may be a lower bound because they use the CCSR model climatology that over the ocean generally underestimates the satellite-derived AOT from AVHRR. We intend to work with next generation of satellite climatology [*Mishchenko et al.*, 2002] that will consolidate ocean and land AOT to reduce this uncertainty.

The monthly mean aerosol climatologies here are used in conjunction with a 3-hour met field of varying cloud layers. Generally, the aerosols have maximal impact on photochemistry in cloud-free conditions. If the cloud fields and aerosols are correlated, then our assumption of constant AOT for variations in cloud cover may induce errors. For AVHRR, the climatology is based on cloud-free conditions, and thus there should be minimal systematic bias in these simulations. Uncertainties in aerosol composition, radiative properties, and vertical distribution all affect tropospheric photolysis. For example, we assume that the aerosol vertical distribution of AVHRR climatology is proportional to the local water vapor density in the CTM. This assumption is perhaps fine for sulfate, but wrong for dust which is generally transported in a dry layer above the boundary layer. The aerosol vertical profiles are the mostly poorly known data in aerosol research. In addition, refractive indices vary with wavelength. Therefore, the wavelength-independent indices adopted in our study, although they well represent the mean values in the key tropospheric chemical spectrum, will induce the error in photolysis calculation. A next step would be to couple a full aerosol model with the tropospheric CTM to resolve issues of variability, and the correlation of anthropogenic aerosols with trace-gas pollutants. We believe that this study demonstrates the necessity for coupled aerosol-chemistry models to use fast-J or an equivalent model that couples aerosols with clouds and ozone in calculating photolysis.

Aerosols also impact tropospheric photochemistry through

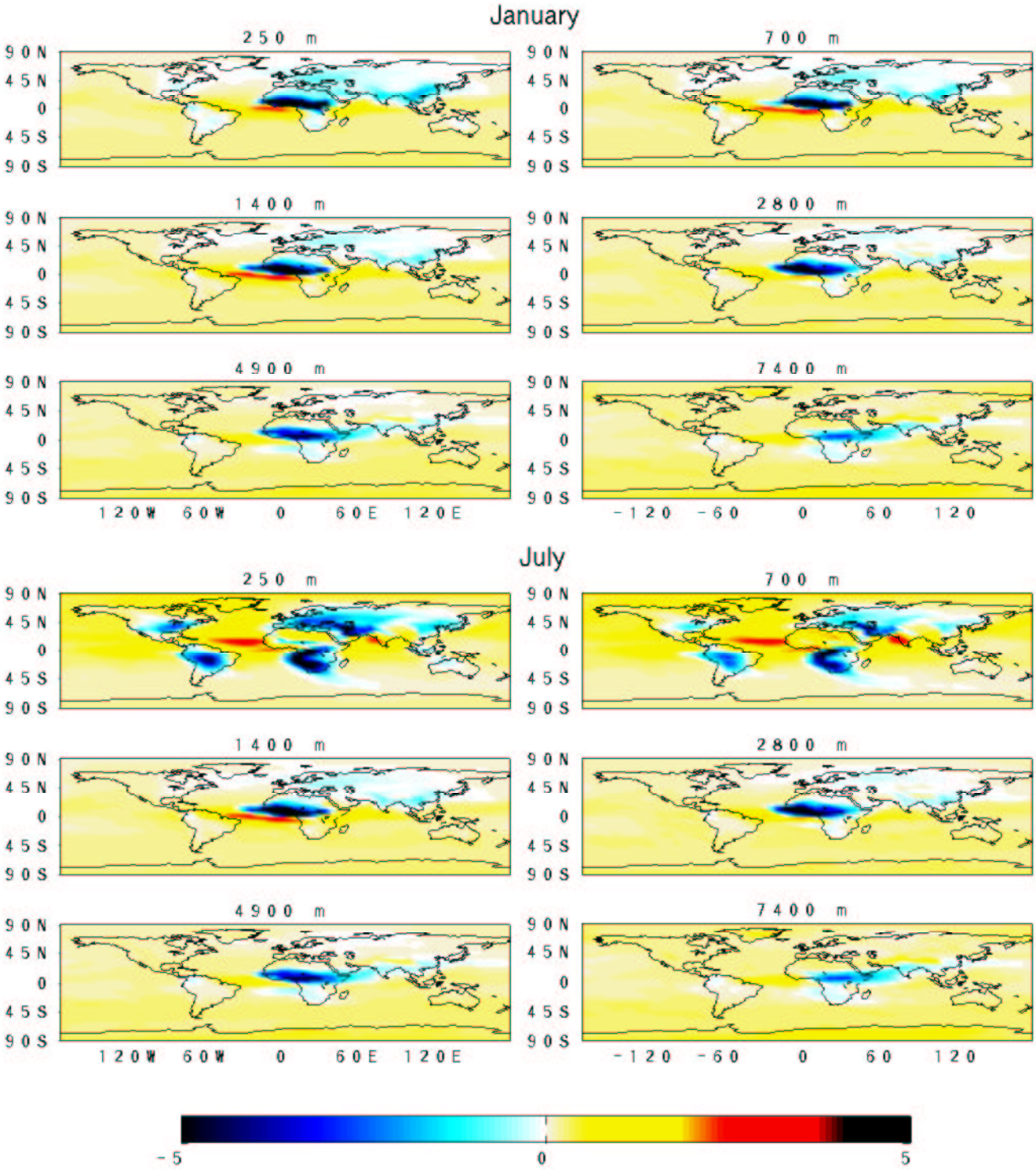

Figure 3. Perturbations to O_3 (ppb) by global aerosol at six atmospheric layers in January and July.

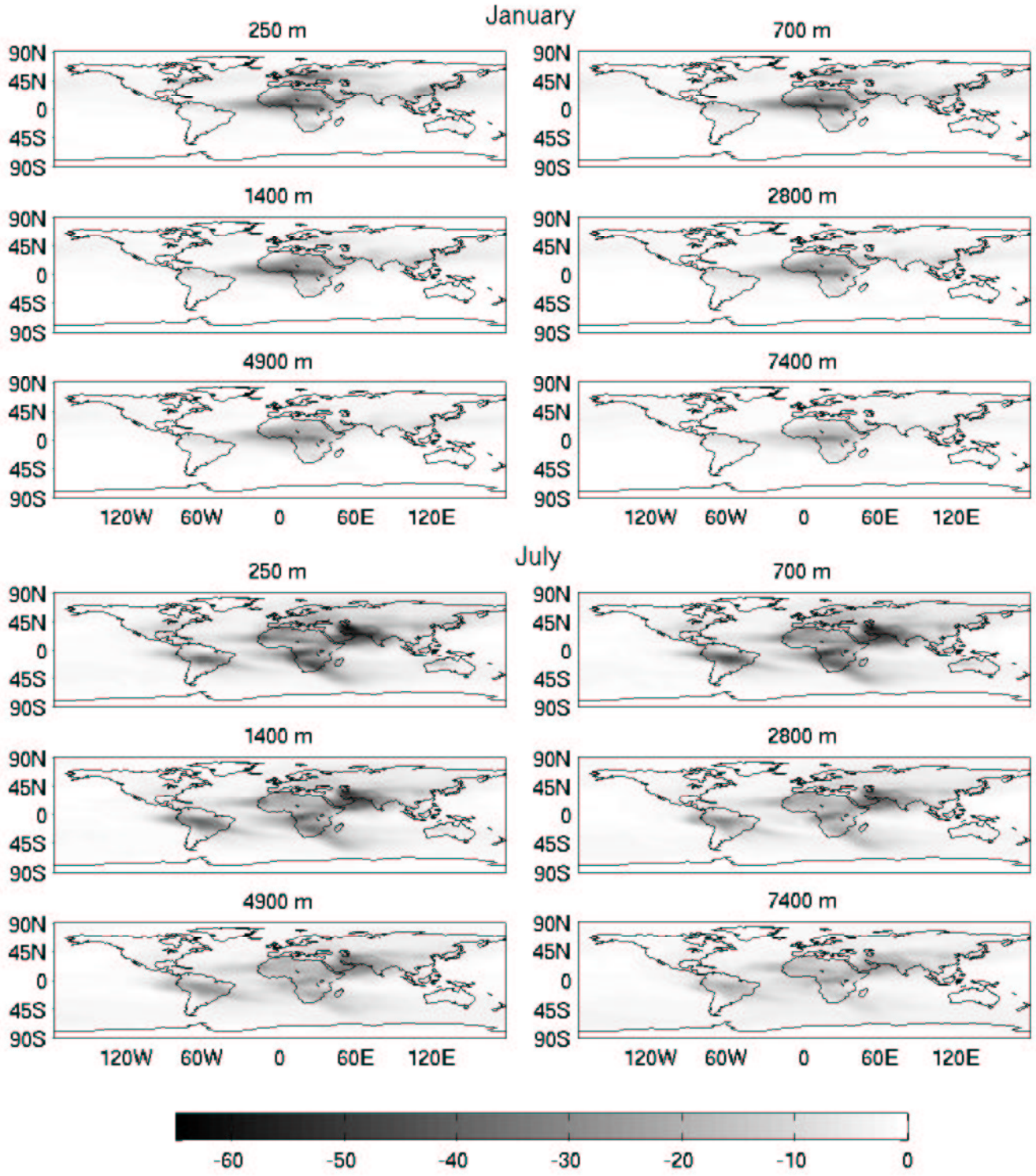

Figure 4. Perturbations to OH (%) by global aerosol at six atmospheric layers in January and July.

Table 3. Sensitivity studies of global mean chemical perturbations based on short-term simulations for July from CCSR (land-plus-ocean and ocean-only) and AVHRR (ocean-only). For AVHRR the standard model is compared with uncertainties in refractive index: moderate dust absorption, moderate and weak carbonaceous absorption, and just sea salt (see text).

global mean	CCSR global	CCSR ocean	AVHRR ocean (std)	AVHRR (mod-D)	AVHRR (mod-C)	AVHRR (weak-C)	AVHRR (sea salt)
O_3	+0.30 DU	+0.13 DU	+0.19 DU	+0.15 DU	+0.09 DU	+0.07 DU	+0.04 DU
NO	-2.4 %	-0.5 %	-1.6 %	-1.6 %	-0.8 %	-0.6 %	-0.4 %
NO_2	+6.5 %	+1.4 %	+2.2 %	+2.2 %	+1.0 %	+0.7 %	+0.3 %
PAN	+9.4 %	+2.9 %	+3.3 %	+3.3 %	+1.5 %	+1.0 %	+0.4 %
OH	-8.1 %	-2.4 %	-4.9 %	-4.9 %	-1.5 %	-0.8 %	-0.3 %

Table 4. Global mean changes in tropospheric chemistry driven by aerosol impacts on photolysis rates. Calculations for the CCSR climatologies for January and July are averaged to estimate the annual change. Additional projected CH_4 feedbacks at steady-state are based on IPCC 2001 and predict that without aerosols CH_4 would be about 130 ppb lower.

global	Jan	Jul	annual	CH_4 feedback	steady-state
CH_4 lifetime	+3.6 %	+7.6 %	+5.6 %	+2.2 %	+7.8 %
mean OH	-3.9 %	-7.9 %	-5.9 %	-2.3 %	-8.2 %
mean O_3	+0.14 DU	+0.36 DU	+0.25 DU	+0.38 DU	+0.63 DU

gas-aerosol (heterogeneous) reactions, and many different types of heterogeneous reactions have been studied [*Dentener and Crutzen*, 1993; *Dentener et al.*, 1996; *Lary et al.*, 1996; *Wahner et al.*, 1998; *Lary et al.*, 1999; *Knipping et al.*, 2000; *Jacob*, 2000; *Tie et al.*, 2001; *Underwood et al.*, 2002]. For example, the impact of aqueous phase reactions of HNO_4 [*Dentener et al.*, 2002] appears to be comparable to the photolytic impacts shown here, although photolytic changes in OH extend throughout most of the troposphere. However, such evaluations are even more uncertain than this one because the detailed chemical composition and mixture of the aerosols, which plays a great role in heterogeneous chemistry, is even more difficult to extract from the observed climatology.

Acknowledgments. We thank the NASA Global Aerosol Climatology Project for its support of this research. We are grateful to the entire GACP team, and particularly M. Mishchenko and I. Geogszhayev for their help with aerosol climatologies and their program to compute optical properties of aerosols. We also thank O. Wild for his helpful comments. This thesis work was also funded by the NASA and NSF atmospheric chemistry programs.

References

Ansmann, A., D. Althausen, U. Wandinger, K. Franke, D. Muller, F. Wagner, and J. Heintzenberg, Vertical profiling of the indian aerosol plume with six-wavelength lider during indoex: a first case study, *Geophys. Res. Lett.*, *27*, 963–966, 2000.

Avallone, L. M., and M. Prather, Tracer-tracer correlations: three-dimensional model simulations and comparison to observations, *J. Geophys. Res.*, *102*, 19233–19246, 1997.

Balis, D. S., C. S. Zerefos, K. Kourtidis, A. F. Bais, A. Hofzumahaus, A. Kraus, R. Schmitt, M. Blumthaler, and G. P. Gobbi, Measurements and modeling of photolysis rates during the PAUR II campaign, *Submitted to J. Geophys. Res.*, 2001.

Bates, T. S., et al., Regional physical and chemical properties of the marine boundary layer aerosol across the atlantic during aerosols99: An overview, *J. Geophys. Res.*, *106*, 20767–20782, 2001.

Benkovitz, C. M., M. T. Scholtz, J. Pacyna, L. Tarrasón, J. Dignon, E. C. Voldner, P. A. Spiro, J. A. Logan, and T. E. Graedel, Global gridded inventories of anthropogenic emissions of Sulfur and Nitrogen, *J. Geophys. Res.*, *101*, 29239–29253, 1996.

Bian, H., Improvement and application of uci chemistry transport model, 2001.

Bian, H., and M. J. Prather, Fast-J2: Accurate simulation of stratospheric photolysis in global chemistry models, *J. Atmos. Chem.*, *41*, 281–296, 2002.

Chin, M., et al., Tropospheric aerosol optical thickness from the GOCART model and comparisons with satellite and sun photometer measurements, *J. Atmos. Sci.*, *59*, 461–483, 2002.

Clarke, A. D., and V. N. Kapustin, A pacific aerosol survey. part i: A decade of data on particle production, transport, evolution, and mixing in the troposphere, *J. Atmos. Sci.*, pp. 363–382, 2002.

Dentener, F. J., and P. J. Crutzen, Reactions of N_2O_5 on tropospheric aerosols: Impact on the global distributions of NO_x, O_3, and OH, *J. Geophys. Res.*, *98*, 7149–7163, 1993.

Dentener, F. J., G. R. Carmichael, Y. Zhang, J. Lelieveld, and P. J. Crutzen, Role of mineral aerosol as a reactive surface in the global troposphere, *J. Geophys. Res.*, *101*, 22869–22889, 1996.

Dentener, F. J., J. Williams, and S. Metzger, Aqueous phase reaction of hno_4: The impact on tropospheric chemistr, *J. Atmos. Chem.*, *41*, 109–134, 2002.

Diaz, J., F. Exposito, C. Torres, F. Herrera, J. Prospero, and M. Romero, Radiative properties of aerosols in Saharan dust outbreaks using ground-based and satellite data: Applications to radiative forcing, *J. Geophys. Res.*, *106*, 18403–18416, 2001.

Dickerson, R. R., S. Kondragunta, G. Stenchikov, K. L. Civerolo, B. G. Doddridge, and B. N. Holben, The impact of aerosols on solar ultraviolet radiation and photochemical smog, *Science*, *278*, 827–830, 1997.

Diner, D. J., et al., Misr aerosol optical depth retrievals over southern africa during the safari-2000 dry season campaigh, *Geophys. Res. Lett.*, *28*, 3127–2130, 2001.

Dubovik, O., B. Holben, T. F. Eck, A. Smirnov, Y. J. Kaufman, M. D. King, D. Tanré, and I. Slutsker, Variability of absorption and optical properties of key aerosol types observed in worldwide locations, *J. Atmos. Sci.*, *59*, 590–608, 2002.

Giorgi, F., and W. L. Chameides, Rainout lifetimes of highly soluble aerosols and gases as inferred from simulation with a general circulation model, *J. Geophys. Res.*, *91*, 14367–14376, 1986.

Grams, G. W., I. Blifford, D. G. Jr., and P. Russell, Complex index of refraction of airborne soil particles, *J. Appl. Meteor.*, *13*, 459–471, 1974.

Hall, T. M., and M. Prather, Simulations of the trend and annual cycle in stratospheric co_2, *J. Geophys. Res.*, *98*, 10573–10581, 1993.

Hannegan, B., S. Olsen, M. Prather, X. Zhu, D. Rind, and J. Lerner, The dry stratosphere: A limit on cometary water influx, *Geophys. Res. Lett.*, *25*, 1649–1652, 1998.

He, S., and G. R. Carmichael, Sensitivity of photolysis rates and ozone production in the troposphere to aerosol properties, *J. Geophys. Res.*, *104*, 26307–26324, 1999.

Higurashi, A., T. Nakajima, B. Holben, A. Smirnov, R. Frouin, and B. Chatenet, A study of global aerosol optical climatology with two-channel avhrr remote sensing, *J. of Climate*, *13*, 2011–2027, 2000.

Holben, B., Web page for aeronet, http://AERONET.gsfc.nasa.gov:8080.

Hook, S. J., J. J. Myers, K. J. Thome, M. Fitzgerald, and A. B. Kahle, The modis/aster airborn simulator (master)- a new instrument for earth science studies, *Remote Sensing of Environment*, *76*, 93–102, 2001.

Hsu, N. C., J. R. Herman, O. Torres, B. N. Holben, D. Tanre, T. F. Eck, A. Smirnov, B. Chatenet, and F. Lavenu, Comparisons of the TOMS aerosol index with Sun-photometer aerosol optical thickness: Results and applications, *J. Geophys. Res.*, *104*, 6269–6279, 1999.

Jacob, D. J., Heterogeneous chemistry and tropospheric ozone, *Atmos. Env.*, *34*, 2131–2159, 2000.

Jacob, D. J., et al., Deposition of ozone to tundra, *J. Geophys. Res.*, *97*, 16473–16479, 1992.

Jacob, D. J., et al., Evaluation and intercomparison of global atmospheric transport models using ^{222}rn and other short-lived tracers, *J. Geophys. Res.*, *102*, 5953–5970, 1997.

Jacobson, M., Studying the effects of aerosols on vertical photolysis rate coefficient and temperature profiles over an urban airshed, *J. Geophys. Res.*, *103*, 10593–10604, 1998.

Ji, Q., S. Tsay, R. Hansell, and P. Piewskie, Smart ground-based radiation measurements during pride, *Tech. rep.*, Eos Trans. AGU, 81(48), Fall Meet. Suppl., Abstract, 2000.

Kaufman, Y., D. Tanre, O. Dubovik, A. Karnieli, and L. Remer, Absorption of sunlight by dust as inferred from satellite and ground-based remote sensing, *Geophys. Res. Lett.*, *28*, 1479–1482, 2001.

Kinne, S., et al., A global comparison among models, satellite data and aeronet ground data, *J. Geophys. Res.*, *in press*, 2002.

Knapp, K. R., and L. L. Stowe, Evaluating the potential for retrieving aerosol optical depth over land from avhrr pathfinder atmosphere data, *J. Atmos. Sci.*, *59*, 279–293, 2002.

Knipping, E. M., M. J. Lakin, P. J. K. J. Foster, D. J. Tobias, R. B. Gerber, D. Dabdub, and B. J. Finlayson-Pitts, Experiments and simulations of ion-enhanced interfacial chemistry on aqueous nacl aerosols, *SCIENCE*, *288*, 301–306, 2000.

Lary, D. J., M. P. Chipperfield, R. Toumi, and T. Lenton, Heterogeneous atmospheric bromine chemistry, *J. Geophys. Res.*, *101*, 1489–1504, 1996.

Lary, D. J., D. E. Shallcross, and R. Toumi, Carbonaceous aerosols and their potential role in atmospheric chemistry, *J. Geophys. Res.*, *104*, 15929–15940, 1999.

McLinden, C. A., S. C. Olsen, B. Hannegan, O. Wild, M. J. Prather, and J. Sundet, Stratospheric ozone in 3-d models: A simple chemistry and the cross-tropopause flux, *J. Geophys. Res.*, *105*, 14653–14665, 2000.

Mishchenko, M. M., aerosol climotology, http://gacp.giss.nasa.gov/.

Mishchenko, M. M., I. Geogdzhayev, B. Cairns, W. Rossow, and A. Lacis, Aerosol retrievals over the ocean by use of channels 1 and 2 avhrr data: sensitivity analysis and preliminary results, *Applied Optics*, *38*, 7325–7341, 1999a.

Mishchenko, M. M., J. Dlugach, E. Yanovitskij, and N. Zakharova, Bidirectional reflectance of flat, optically thick particulate layers: an efficient radiative transfer solution and applications to snow and soil surfaces, *J. of Quanti. Spectoscopy & Radiative Transfer*, *63*, 409–432, 1999b.

Mishchenko, M. M., L. D. Travis, and A. A. Lacis, *Scattering, Absorption, and Emmision of Light by Small Particles*, Cambridge University Press, 2002.

Olsen, S. C., B. Hannegan, X. Zhu, and M. Prather, Evaluating ozone depletion from very short-lived halocarbons, *Geophys. Res. Letters*, *27*, 1475–1478, 2000.

Olson, J., et al., Results from the Intergovernmental Panel on Climatic Change Photochemical Model Intercomparison (PhotoComp), *J. Geophys. Res.*, *102*, 5979–5991, 1997.

Penner, J. E., et al., A comparison of model- and satellite-derived aerosol optical depth and reflectivity, *J. Atmos. Sci.*, *59*, 441–460, 2002.

Prather, M. J., and D. Ehhalt, Atmospheric chemistry and greenhouse gases, in *Climate Change 2001, the Scientific Basis*, edited by J. e. a. Houghotn, pp. 239–288, Cambridge Unversity Press, 2001.

Prather, M. J., M. MeElroy, S. Wofsy, G. Russell, and D. Rind, Chemistry of the global troposphere: Fluorocarbon as tracers of air motion, *J. Geophy. Res.*, *92*, 6579–6613, 1987.

Savoie, D. L., H. Maring, M. Izaguirre, T. Snowdon, and L. Custals, Ground-based measurements of aerosol chemical, physical, and optical properties during the Puerto Rico Dust Experiment (PRIDE), in *Eos, Transactions*, vol. 81, p. F44, American Geophysical Union, 2000.

Stowe, L. L., A. M. Ignatov, and R. R. Singh, Development, validation, and potential enhancements to the second-generation operational aerosol product at the National Environmental Satellite, Data, and Information Service of the National Oceanic and Atmospheric Administration, *J. Geophys. Res.*, *102*, 16923–16934, 1997.

Takemura, T., H. Okamoto, Y. Maruyama, A. Numaguti, A. Higurashi, and T. Nakajuma, Global three-dimensional simulation of aerosol optical thickness distribution of various origins, *J. Geophys. Res.*, *105*, 17853–17873, 2000.

Takemura, T., T. Nakajima, O. Dubovik, B. N. Holben, and S. Kinne, Single-scattering albedo and radiative forcing of various aerosol species with a global three-dimensional model, *J. Climate*, pp. 333–352, 2002.

Tie, X., G. Brasseur, L. Emmons, L. Horowitz, and D. Kinnison, Effects of aerosols on tropospheric oxidants: A global model study, *J. Geophys. Res.*, *106*, 22931–22964, 2001.

Torres, O., P. K. Bhartia, J. R. Herman, A. Sinyuk, P. Ginoux, and B. Holben, A long-term record of aerosol optical depth from TOMS observations and comparison to AERONET measurements, *J. Atmos. Sci.*, *59*, 398–413, 2002.

Twitty, J. T., and J. Weinman, Radiative properties of carbonaceous aerosols, *J. Appl. Meteor.*, *10*, 725–731, 1971.

Underwood, G. M., C. H. Song, M. Phadnis, G. R. Carmichael, and V. H. Grassian, Heterogeneous reactions of NO_2 and HNO_3 on oxides and mineral dust: A combined laboratory and modeling study, *J. Geophys. Res.*, *106*, 18055–18066, 2002.

Volz, F. E., Infrared refractive index of atmospheric aerosol substances, *Appl. Optics*, *11*, 755–759, 1972.

Wahner, A., T. F. Mentel, M. Sohn, and J. Stier, Heterogeneous reaction of n_2o_5 on sodium nitrate, *J. Geophys. Res.*, *103*, 31103–31112, 1998.

Ward, G., K. Cushing, R. McPeters, and A. Green, Atmospheric aerosol index of refraction and size-altitude distribution from bistatic laser scattering and solar aureole measurements, *Appl. Optics*, *12*, 2585–2592, 1973.

Wild, O., and H. Akimoto, Intercontinental transport of ozone and its precursors in a global ctm, *J. Geophys. Res.*, *106*, 27729–27744, 2001.

Wild, O., and M. Prather, Excitation of the primary tropospheric chemical mode in a global ctm, *J. Geophys. Res.*, *105*, 24647–24660, 2000.

Wild, O., X. Zhu, and M. Prather, Fast-J: Accurate simulation of in- and below-cloud photolysis in tropospheric chemical models, *J. Atmos. Chem.*, *37*, 245–282, 2000.

H. Bian, M. J. Prather, Department of Earth System Science, University of California, Irvine, CA 92697-3100. (hbian@uci.edu and mprather@uci.edu)

T. Takemura, Research Institute for Applied Mechanics, Kyushu University, Fukuoka, Japan, 6-1 Kasuga-koen, Kasuga, Fukuoka 816-8580, Japan. (toshi@riam.kyushuu.ac.jp)

Received Month Day, 2002; revised Month Day, 2002; accepted Month Day, 2002.